

---

# QUIK: TOWARDS END-TO-END 4-BIT INFERENCE ON GENERATIVE LARGE LANGUAGE MODELS

---

Saleh Ashkboos<sup>\*1</sup> Ilia Markov<sup>\*2</sup> Elias Frantar<sup>2</sup> Tingxuan Zhong<sup>3</sup> Xingchen Wang<sup>3</sup> Jie Ren<sup>4</sup>  
Torsten Hoefler<sup>1</sup> Dan Alistarh<sup>2,5</sup>

## ABSTRACT

Large Language Models (LLMs) from the GPT family have become extremely popular, leading to a race towards reducing their inference costs to allow for efficient local computation. Yet, the vast majority of existing work focuses on weight-only quantization, which can reduce runtime costs in the memory-bound one-token-at-a-time generative setting, but does not address them in compute-bound scenarios, such as batched inference or prompt processing. In this paper, we address the general quantization problem, where both weights and activations should be quantized. We show, for the first time, that the majority of inference computations for large generative models such as LLaMA, OPT, and Falcon can be performed with both weights and activations being cast to 4 bits, in a way that leads to practical speedups, while at the same time maintaining good accuracy. We achieve this via a hybrid quantization strategy called QUIK, which compresses most of the weights and activations to 4-bit, while keeping some outlier weights and activations in higher-precision. The key feature of our scheme is that it is designed with computational efficiency in mind: we provide GPU kernels matching the QUIK format with highly-efficient layer-wise runtimes, which lead to practical end-to-end throughput improvements of up to 3.4x relative to FP16 execution. We provide detailed studies for models from the OPT, LLaMA-2 and Falcon families, as well as a first instance of accurate inference using quantization plus 2:4 sparsity. Code is available at: <https://github.com/IST-DASLab/QUIK>.

## 1 INTRODUCTION

Large language models (LLMs) from the Generative Pre-trained Transformer (GPT) family (Radford et al., 2019) are massively popular. One key contributor to their adoption has been the ability to compress them using advanced techniques, e.g., (Frantar et al., 2022; Dettmers et al., 2022; Lin et al., 2023; Yuan et al., 2023), enabling local storage and efficient generative inference for these models, even on personal computers. The vast majority of work on LLM quantization can be categorized into two cases:

- *Weight-only quantization methods* (Frantar et al., 2022; Dettmers et al., 2022; Lin et al., 2023; Dettmers et al., 2023; Lin et al., 2023; Kim et al., 2023) that help reduce the massive memory-transfer costs of LLM inference. Yet, these methods do not reduce computation, and cannot provide significant speedup for computationally-bound

settings, such as prompt processing or batch inference.

- *Joint weight-activation quantization methods*, which can provide computational improvements, but either focus exclusively on 8-bit weights and activations (8W8A) (Xiao et al., 2022; Dettmers et al., 2022), or execute with large amounts of accuracy loss relative to their uncompressed counterparts (Yuan et al., 2023; Shao et al., 2023).

Thus, there is still a significant gap between compressed formats efficiently supported by hardware—specifically, NVIDIA GPUs natively support accelerated 4bit matrix multiplication on both the Ampere and Lovelace architectures (NVIDIA, 2023)—and quantization algorithms with computational support which would allow inference to be performed accurately on such compressed formats.

**Contribution.** In this paper, we take a step towards bridging this gap, and show for the first time that a large fraction of the computation in modern LLMs such as OPT (Zhang et al., 2022), LLaMA-2 (Touvron et al., 2023) and Falcon (TII UAE, 2023) can be performed accurately and efficiently using *4-bit activations and weights (4W4A)*.

On the algorithmic side, we show significantly improved results relative to prior work on joint quantization of weights and activations to 4 bits, via a hybrid scheme for

<sup>\*</sup>Equal contribution <sup>1</sup>ETH Zurich <sup>2</sup>Institute of Science and Technology Austria <sup>3</sup>Xidian University <sup>4</sup>KAUST <sup>5</sup>Neural Magic, Inc.. Correspondence to: Saleh Ashkboos <saleh.ashkboos@inf.ethz.ch>, Dan Alistarh <dan.alistarh@ist.ac.at>.

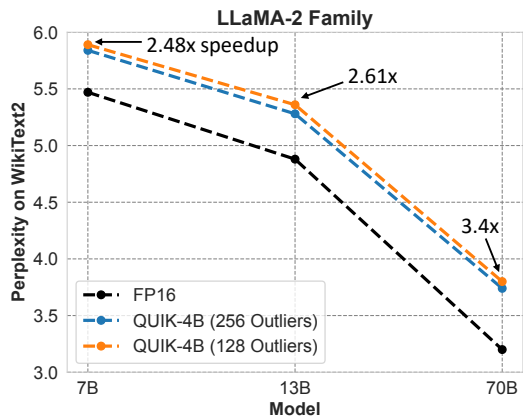


Figure 1. Accuracy and speedups for QUIK at different model sizes, on the LLaMA family of models. QUIK achieves up to 3.4x speedup with minor accuracy degradation on LLaMA-2 models.

**QU**antization to INT4 with GPU **K**ernel support, called **QUIK**. In QUIK, matrices are split into “base” weights and activations, which are processed exclusively at 4-bit precision, and a small number of “outlier” weights and activations, which are processed at higher precision such as INT8 or FP16. Using this approach, as well as additional insights into layer sensitivity, we build a framework which can recover accuracy within 0.3–0.5 perplexity points across model sizes (corresponding to 6%–16% relative error), while executing a large fraction of the inference in INT4. For illustration, for the sensitive LLaMA2 model with 70B parameters, we can recover accuracy within 0.5 perplexity, while executing 70% of the linear layer computations in INT4, leading to 3.4x end-to-end speedups (see Figure 1).

On the systems side, the key feature of QUIK is that it can be implemented efficiently via GPU kernels with low runtime and memory overheads relative to GPU-native INT4 matrix multiplication (MatMul). We demonstrate this via a general implementation leading to per-layer speedups and end-to-end throughput improvements relative to both FP16 and INT8 baselines. Specifically, we show that supporting a limited number of feature and weight outliers can have negligible overhead by fusing the quantization and dequantization operations into the MatMul and by mitigating their costs in linear layers via additional optimizations.

Overall, QUIK leverages quantization for significant end-to-end speedups and memory reductions. For example, for processing a sequence of 2048 tokens on a commodity RTX 3090 GPU, we achieve end-to-end speedups between 3.1x, for the OPT-66B and Falcon-180B models, and 3.4x for LLaMA2-70B, relative to a theoretical optimum of  $\approx 4x$ . In addition, QUIK requires much less GPU memory, and therefore, less GPUs, relative to FP16. For instance, QUIK provides 3.6x memory reduction for OPT-66B, and 3x com-

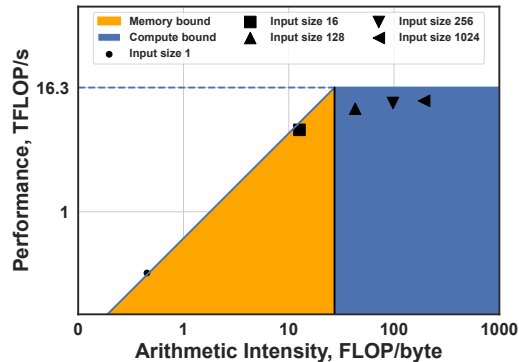


Figure 2. Roofline analysis of a standard LLM MatMul operation, for a matrix of size 8K x 8K, in FP32, on an NVIDIA GPU. Markers denote the results of profiling with different token counts (from 1 to 1024). Small counts (1 and 16) are memory-bound, whereas larger counts (from 128 to 1024) are compute-bound.

pression for accurate execution of LLaMA2-70B, executing the latter in less than 50GB of GPU memory.

## 2 MOTIVATION

**Roofline Analysis.** To motivate our focus on the compute-bound case, we begin an analysis of the basic computational operation in the context of LLMs, a matrix multiplication for different numbers of tokens. We profile a linear layer of standard size (11K x 4K, corresponding to the MLP in LLaMA-7B (Touvron et al., 2023)), using the NVIDIA NSight Compute toolkit (NVIDIA), from a single token to 16, 256 and 1024 tokens.

The results, illustrated in Figure 2, clearly show that the case of few tokens (1 and 16) is memory-bound, whereas the workload becomes compute-bound for the larger token counts, specifically larger than 128. A realistic end-to-end LLM deployment would need to consider optimizing both scenarios, as the prompt processing “prefill” case falls into the large token count scenario, whereas generating one-token-at-a-time falls into the former case. Moreover, running a “batched” version of the single-token workload, i.e. for multiple users, would again result in large token counts, returning to the compute-bound case.

Further, we observe that existing methods for weight-only quantization, e.g. (Frantar et al., 2022; Dettmers & Zettlemoyer, 2022; Lin et al., 2023) only serve to improve the arithmetic intensity of this operation, by reducing the amount of data which needs to be transferred per operation, but still perform the computation in the original precision. Thus, they do not help in the compute-bound case, and in fact even *slightly increase* the amount of computation per operation, due to the de-quantization overheads.

**Speedup Potential.** Given our focus on the compute-bound

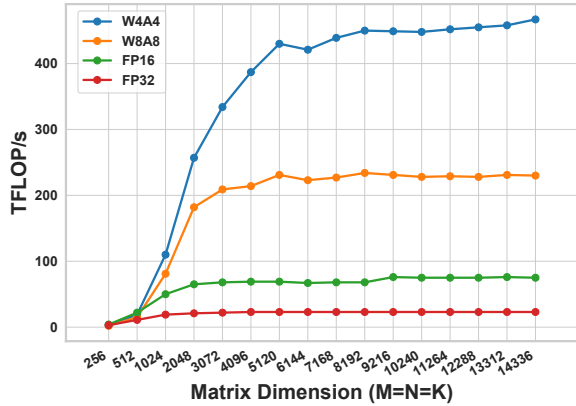


Figure 3. Ideal matrix multiplication performance for different layer sizes and data precision on RTX3090.

case, it is natural to investigate the available hardware options leading to potential speedups. As shown in Figure 3, quantization is a natural approach in this case, given that NVIDIA GPUs have native support for INT4 and INT8 data types, providing major throughput improvements across matrix sizes. Specifically, INT8 provides throughput improvements that can be slightly higher than 2x relative to FP16 on raw MatMuls, whereas INT4 almost doubles over INT8. However, to leverage these hardware operations, *both layer inputs (activations) and layer weights* must be quantized to the same compressed data type.

We will focus on accurate post-training quantization for LLM inference, by compressing both weights and activations, primarily to INT4 data types. As stated, weight-only quantization (Frantar et al., 2022; Lin et al., 2023) does not transfer to our setting, and activation quantization is notoriously challenging (Xiao et al., 2022). Moreover, as shown in Table 1, existing methods for quantizing both weights and activations in LLMs break down in terms of accuracy when applied to 4bit compression.

## 3 METHOD

### 3.1 Background

We focus on the task of accelerating linear layers within Large Language Models (LLMs) by employing 4-bit quantization for both the weight matrix  $\mathbf{W}$  and the input matrix  $\mathbf{X}$ . Following the PyTorch definition (Paszke et al., 2019), a linear layer carries out a linear transformation along with a bias vector  $\mathbf{b}$ , taking the form of  $\mathbf{X}\mathbf{W}^T + \mathbf{b}$ . We now describe the background and details of the technique.

**Outliers in Input Quantization.** It is known that the activation matrices are hard to quantize (Dettmers et al., 2022; Xiao et al., 2022; Yuan et al., 2023), mainly due to the presence of *outlier features* in these matrices, where some of

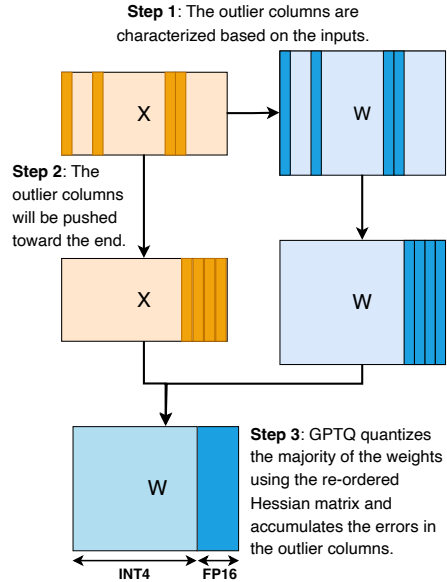


Figure 4. Outlier-aware quantization with QUIK. Outlier weight columns are extracted based on outlier columns in the input. We permute the outlier columns toward the end of the matrix before applying GPTQ quantization (using the re-ordered Hessian matrix) to accumulate the quantization errors in the FP16 columns.

the columns have up to 100x larger magnitudes. LLM.int8() (Dettmers et al., 2022) identifies and extracts the outlier columns of  $\mathbf{X}$  during the forward pass and quantizes the rest of the elements with 8-bit. However, LLM.int8() is not efficient at runtime due to the added computational cost of determining outliers on-the-fly. Recent work (Xiao et al., 2022) has shown that the outlier features are fixed for each layer across datasets, which means that we can extract outlier indices offline using a small calibration set.

**GPTQ Weight Quantization.** GPTQ (Frantar et al., 2022) is a weight-only quantization method which involves the quantization of  $\mathbf{W}$  while retaining the activations  $\mathbf{X}$  in FP16. To do this, it iterates over the weight columns; for each column, it quantizes all of its elements simultaneously. Following the quantization of a weight column, GPTQ adjusts the remaining unquantized columns, to the right of the current one, by using second-order information to compensate for the introduced quantization error in the current step. This process *accumulates the quantization errors at the last columns*, making them more sensitive to quantization.

### 3.2 QUIK Quantization

**Overview.** At a high level, QUIK works as follows. First, note that, during the linear transformation  $\mathbf{X}\mathbf{W}^T$ , the outlier columns in  $\mathbf{X}$ , by which we mean the columns with large average values defined previously, will always be multiplied by certain columns in  $\mathbf{W}^T$ , as illustrated in Figure 4. We

leverage this observation to improve the quality of GPTQ quantization, in a setting where we quantize (part of) the activations as well.

Since the outlier columns are fixed across datasets, we begin by extracting the indices of the outlier columns by means of a calibration set. Then, we rearrange the weight columns (and their corresponding input columns), to shift the outliers toward the end. Finally, we perform quantization on the weight columns up to the index of the outliers. This circumvents quantization of these “difficult” columns. It also helps GPTQ quantization by 1) aggregating the quantization errors to the columns we keep in FP16, and 2) removing potential weight outliers from the 4bit quantization scale.

**Weight Clipping.** Weight clipping improves quantization by trimming the input distribution before rounding. This could be done by either training the whole network to find the optimal clipping thresholds (Shao et al., 2023; Esser et al., 2019; Choi et al., 2018); or employing heuristic methods (Lin et al., 2023; Lee et al., 2023; Kim et al., 2023). We found that applying linear search over the clipping thresholds for weight quantization improves final perplexity.

**Sensitivity-Based Partial Quantization.** Accurately selecting outlier columns is key for QUIK. Following (Xiao et al., 2022; Dettmers et al., 2022), we select the columns with the largest  $\ell_\infty$  norm as outliers. Since finding these columns dynamically at runtime is costly, we follow (Xiao et al., 2022) in identifying a predefined set of outliers for each layer via a calibration set (see Section 4), and quantize the weights offline. We use the same outlier indices for extracting the input outlier columns during the forward pass.

This approach is sufficient for accurate quantization of models such as OPT (Zhang et al., 2022) (see Section 4). However, highly-accurate massive models such as LLaMA2-70B present a further challenge due to their FeedForward layers, which involve three linear transformations along with element-wise multiplication, as well as the use of the Sigmoid Linear Unit (SiLU) activations. Specifically, our  $\ell_\infty$  norm analysis illustrated in Figure 10, suggests that the  $\text{Down}_{\text{proj}}$  layers are much more sensitive to quantization. (Li et al. (2023) arrived at a similar observation.) Thus, we extend our scheme to recover accuracy by quantizing the  $\text{Down}_{\text{proj}}$  layers to 8 bits instead of 4, without other changes to our method. We illustrate the outlier selection procedure in detail in Section 4.3.1. Figure 11 presents a detailed analysis of the overall FLOP breakdown to various precisions when quantizing the LLaMA2-70B model via QUIK.

### 3.3 Efficient Inference Implementation

We now provide a high-level description of how models in the QUIK format are executed efficiently on GPU. We illustrate the workflow in Figure 5 and provide pseudocode

in Algorithm 1. The first and most important step in QUIK is splitting the input matrix of shape (#tokens, #features) column-wise, so across features, into two sub-sets, a small “full precision” part (usually half or bfloat16) and a large base part, which will be quantized (see line 3 in the pseudocode). The full-precision part is multiplied with the corresponding (full-precision) part of the weight matrix in standard fashion, while the rest goes through the quantized matrix multiplication pipeline described next.

The quantized MatMul pipeline consists of three parts: 1) dynamically quantizing the activations, 2) actually performing the MatMul of quantized activations and weights, and 3) dequantizing the result back to floating point format.

**Quantization.** In general, we quantize weights *symmetrically* (only scale) per output and quantize activations *asymmetrically* (scale and zero) per token. The former is done *offline* (see Section 3.2), while the latter must be done *online* based on the current activation values. Specifically, we first scan the activations to determine the per-token min- and max-value, from which we calculate the scale and zero point (line 12). These are then used to turn the floating point activations into integers, which are written out again as signed (hence the halfRange subtraction in line 14) INT4 or INT8 values in a packed format for efficient further processing (see lines 13-16).

**Matrix Multiplication.** The actual MatMul is performed by the CUTLASS (NVIDIA, 2023) library, which is able to effectively utilize the hardware’s INT8/INT4 tensor-cores to perform fast low-precision calculations, while accumulating results in a wider INT32 format.

**Dequantization.** As the MatMul was carried out purely with quantized INT values, we need to convert back to a floating point format in order to properly integrate scale and zero information. Concretely, we need to multiply each output element  $o_{ij}$  by its corresponding input token scale  $\text{scaleAct}$  and output weight scale  $\text{scaleWeight}$  (line 22). Additionally, we also need to account for the activation zero-point  $\text{zeroAct}$ . To do this, we consider a scalar product  $\langle w, x \rangle$  (representing a single output value in our overall matmul) where a constant  $z$  is added to each  $x_i$ :

$$y = \sum_i w_i(x_i + z) = \sum_i w_i x_i + z \cdot \sum_i w_i. \quad (1)$$

Consequently, we must shift by  $z$  times the *sum over relevant weights*, the latter of which is static and can thus be precomputed as  $w_{\text{Reduced}}$ ; the signed to unsigned INT conversion must be considered as well (lines 23 - 24). Finally, we add these dequantized values to the original outlier result, yielding the final output (line 8).



**Algorithm 1** Quantization and Dequantization kernels.

```

1: function QUIK Matmul
2:   Input: wInt, wFP, x, FPindices, scaleWeight, wReduced;
3:   xFP, xQ  $\leftarrow$  split(x, FPindices);
4:   xINT, zeroAct, scaleAct  $\leftarrow$  Quantization(xQ);
5:   resultFP  $\leftarrow$  FPmatmul(xFP, wFP);
6:   resultInt  $\leftarrow$  INTmatmul(xInt, wInt);
7:   dequantFP  $\leftarrow$  Dequantization(resultInt, zeroAct,
   scaleAct, scaleWeight, wReduced)
8:   return dequantFP + resultFP;
9: end function
10: function Quantization
11:   Input: dataFP;
12:   zeroAct, scaleAct  $\leftarrow$  findZeroScale(dataFP);
13:   for elem  $\in$  dataFP, outElem  $\in$  output do
14:     // Use scale/zero corresponding to token
15:     outFP  $\leftarrow$  (elem - zeroAct) / scaleAct - halfRange;
16:     outElem  $\leftarrow$  pack(outFP);
17:   end for
18:   return output, zeroAct, scaleAct;
19: end function
20: function Dequantization
21:   Input: inputINT, zeroAct, scaleAct, scaleWeight, wReduced
22:   for elem  $\in$  inputINT, outElem  $\in$  outputFP do
23:     // Use scales for token and weight row, respectively
24:     x  $\leftarrow$  elem * scaleAct * scaleWeight;
25:     shift  $\leftarrow$  zeroAct + halfRange * scaleAct;
26:     shift  $\leftarrow$  shift * wReduced;
27:     outElem  $\leftarrow$  x + shift;
28:   end for
29:   return outputFP;
30: end function

```

**3.4 Performance Optimizations**

The computational backbone of the QUIK kernel implementation is the low-precision CUTLASS matrix multiplication. However, the mixed precision nature of the algorithm imposes the use of auxiliary functions, such as input data splitting, metadata computation, quantization and dequantization. This provides opportunities for optimizations.

**Quantization Fusion.** A naive implementation of the splitting and quantization pipeline would require one read-and-write pass for the outlier-part, another read-and-write pass for the base-part, two read passes to determine per-token min-max values and one more read-and-write pass for actually carrying out quantization. Many of these slow memory-bound operations can be optimized away via careful operator fusion in the form of bespoke kernels.

Specifically, we assign each input row to a CUDA block and perform 3 passes over it: reduction (finding meta information) over the non-outliers elements, quantization of the non-outliers and moving the outliers to a separate piece of memory. This eliminates two costly read (min-max calcula-

tion and base-part splitting) and one write pass (base-part splitting), and overheads of additional kernel launches.

**Parallelization Tuning.** For the above quantization procedure to be efficient on a modern GPU, we have to ensure optimal parallelization via careful tuning of CUDA blocks and threadcounts. The most critical tuning parameter is the number of rows we process with one CUDA block. Mapping one block per each row brings additional launching overheads, while mapping too many rows per block results in block over-subscription and lower occupancy of the GPU. Hence, we optimized the appropriate number of rows per block for different matrix sizes (usually values between 8 and 32). This improved quantization speed by up to 30%.

**Dequantization Epilogue.** CUTLASS first accumulates MatMul results in registers before committing them to (slow) global memory. We can avoid an unnecessary write and read pass of intermediate INT32 matmul results by directly performing dequantization in a custom *epilogue* that is applied before the global memory commit, which we further directly accumulate into the results of the outlier MatMul. Overall, this interleaves two expensive operations and saves additional kernel launches and memory trips.

**Performance Impact.** To illustrate the impact of these optimizations, we mark them as different versions of our kernel: version 1 has unfused quantization and dequantization; version 2 has fused quantization and unfused dequantization; version 3 fuses both quantization and dequantization.

Figure 6 provides a detailed breakdown of the results of each of these optimizations. We observe that they are especially effective for the small matrix sizes, where they lead to end-to-end speedups of almost 2x. Fused quantization optimization gives up to 40% throughput improvement and the dequantization epilogue yields an additional 10% speedup.

**4 EXPERIMENTAL VALIDATION**

**General setup.** We evaluate our method on OPT (Zhang et al., 2022), LLaMA-2 (Touvron et al., 2023), and Falcon (TII UAE, 2023) models, using HuggingFace (Wolf et al., 2019) implementations of model definitions and datasets. Following SmoothQuant (Xiao et al., 2022), we extract outlier indices using 512 random sentences from the Pile dataset (Gao et al., 2020). We consider up to 5% (based on the model size) of the input features as outliers in the linear layers. During the GPTQ weight quantization, we randomly select 128 samples with 2048 sequence length from the C4 dataset (Raffel et al., 2020). We apply symmetric quantization to weights and asymmetric quantization to activations. Clipping thresholds for weight quantization are found via a linear search over the squared error. Our scheme quantizes a 70B model in less than 2 hours on a single NVIDIA A100 GPU.

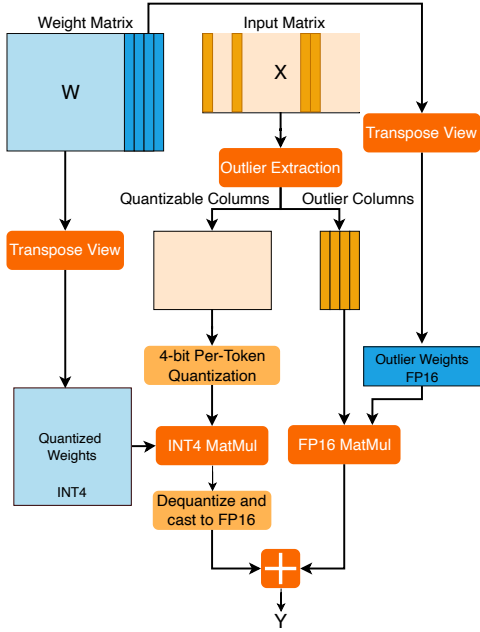


Figure 5. Schematic for the forward pass of a linear layer ( $XW^T$ ) with QUIK-4B. In the first step, the input outlier features are extracted based on the pre-defined indices and the rest of the input values will be quantized using per-token quantization. The INT4 MatMul will be applied using the quantized weights, calculated offline (see Figure 4). Finally, the output will be dequantized, cast to FP16, and added to the result of FP16 MatMul.

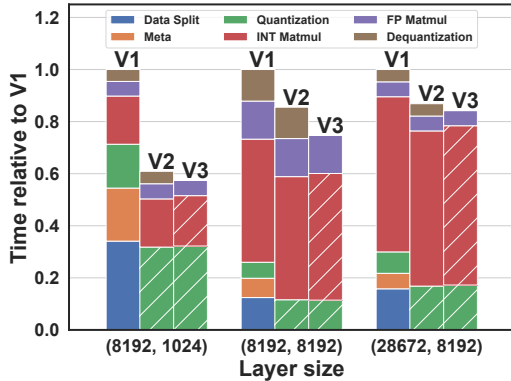


Figure 6. Operation timings in different QUIK-4B versions with 256 outliers relative to the first version for different matrix sizes. Hatched bars represent fused operations. Experiment executed with input size 2048 on an RTX3090 GPU.

#### 4.1 Accuracy Recovery

**Accuracy Comparison on OPT.** We first compare the accuracy of QUIK with prior 4W4A quantization methods: SmoothQuant (Xiao et al., 2022), RPTQ (Yuan et al., 2023) and OmniQuant (Shao et al., 2023).

Table 1 shows the results of all methods for 4 larger OPT models on the WikiText2 task (Merity et al., 2016). We observed that, with QUIK, the accuracy of OPT models

Model	OPT			
	6.7B	13B	30B	66B
Baseline	10.86	10.13	9.56	9.34
SmoothQuant	1.8e4	7.4e3	1.2e4	2.2e5
RPTQ	17.83	17.83	11.50	11.16
OmniQuant	12.24	11.65	10.60	10.29
QUIK (ours)	<b>11.18</b>	<b>10.78</b>	<b>10.08</b>	<b>9.66</b>

Table 1. Perplexity of 4-bit OPT models on the WikiText2 dataset. SmoothQuant, RPTQ, and OmniQuant results are taken from Shao et al. (2023), RPTQ denotes their improved numbers. Note that for the 66B model, all prior schemes keep 0.71% of the linear layer operations in FP16 (the Head), while, by excluding outliers from quantization, we retain 2.78% of operations in FP16.

remains consistent even when employing a uniform number of outliers for all layers (instead of using a percentage of the input features). Consequently, we employed 256 outliers across all linear modules (which is  $\approx 3\%$  of OPT-66B’s hidden size). As can be seen, by effectively leveraging a small amount of full-precision outlier columns, QUIK can significantly outperform prior 4-bit methods, dropping only 0.3 to 0.5 points in perplexity relative to the full precision baseline. We emphasize that, for a fair comparison, QUIK quantizes *all* linear backbone layers to 4-bit here. Additional results are presented in Appendix A.

**Accuracy on LLaMA-2 and Falcon Models.** Next, we move to LLaMA-2 and Falcon models. See Table 2 for the results on WikiText2. As can be seen, QUIK-4B can preserve the accuracy in all models with at most 0.5 perplexity loss for the LLaMA-2 models, and 0.3 for Falcon models.

Model	LLaMA-2			Falcon		
	7B	13B	70B	7B	40B	180B
Baseline	5.47	4.88	3.20	6.59	5.23	3.30
SmoothQuant	83.12	35.88	-	-	-	-
OmniQuant	14.26	12.30	-	-	-	-
QUIK-4B	<b>5.84</b>	<b>5.28</b>	<b>3.74</b>	<b>6.90</b>	<b>5.46</b>	<b>3.61</b>

Table 2. Perplexity results of QUIK for 4-bit LLaMA-2 and Falcon models on WikiText2. We use 256 outliers for all linear layers. For the down-projection (in LLaMA-2 models) and FC2 layers (in Falcon models), we use 8-bit quantization, and increase the number of outliers (in FP16) proportionally to the number of input features of these layers (which is not the case for other schemes). Results for SmoothQuant and OmniQuant follow Shao et al. (2023). OmniQuant does not present results for the Falcon family and LLaMA2-70B in 4-bit. RPTQ does not present any results for LLaMA-2 and Falcon families.

**Zero-Shot Accuracy.** Next, we evaluate the impact of QUIK on the accuracy of zero-shot tasks. To this end, we study the average accuracy of the largest LLaMA-2 and OPT models on five popular zero-shot tasks: PIQA (Tata & Patel, 2003); WinoGrande (Sakaguchi et al., 2021); HellaSwag

**QUIK: Towards End-to-end 4-Bit Inference on Generative Large Language Models**

Model	Bits	Arc Challenge	Arc Easy	HellaSwag	PIQA	WinoGrande	Avg. Score
OPT-30B	FP16	38.05	65.36	72.28	78.13	68.43	64.45
	QUIK-4B	36.69	64.39	70.84	77.75	67.01	63.34
OPT-66B	FP16	40.02	67.26	74.87	79.82	68.82	66.16
	QUIK-4B	38.82	64.73	73.68	79.43	68.82	65.10
LLaMA2-13B	FP16	48.98	77.44	79.38	80.52	72.22	71.70
	QUIK-4B	48.04	74.92	78.36	79.22	71.90	70.49
LLaMA2-70B	FP16	57.34	80.98	83.81	82.75	77.98	76.57
	QUIK-4B	56.14	79.00	81.57	81.56	76.56	74.97

Table 3. LM eval harness results of QUIK on OPT, LLaMA-2, and Falcon families. using 256 outliers.

(Zellers et al., 2019); Arc (Easy and Challenge) (Boratko et al., 2018). We use the LM Evaluation Harness (Gao et al., 2021) with default parameters in our experiments. Table 3 shows the averaged accuracy of QUIK over zero-shot tasks. Similar to the generation task, QUIK preserves the accuracy of zero-shot tasks with at most a 1.5% accuracy drop for LLaMA-2 models and 1.1% for OPT models.

**8-Bit Quantization.** We compare the accuracy of QUIK-8B with SmoothQuant (Xiao et al., 2022) on OPT, LLaMA-2, and Falcon. We use asymmetric per-token quantization for activations and symmetric quantization for the weights in SmoothQuant (these are the same basic settings as for QUIK). Table 4 shows that although both schemes are close to lossless in terms of perplexity difference to FP16, QUIK produces higher accuracy results in most cases, compared to SmoothQuant. Further, it is unclear whether SmoothQuant can be applied to models with *parallel attention*, such as the Falcon-7B model, where the MLP and Attention blocks share the same layer norm for their input, as this prevents scale factor fusion. See Appendix C for further results.

Table 4. Accuracy results for 8-bit models on WikiText2. We use 256 outliers in QUIK experiments. Following the SmoothQuant paper, we use  $\alpha = 0.8$  for LLaMA-2 models and  $\alpha = 0.5$  for OPT and Falcon families.

Model	OPT		LLaMA-2		Falcon	
	30B	66B	13B	70B	40B	180B
FP16	9.56	9.34	4.88	3.20	5.23	3.30
SmoothQuant	9.59	9.80	4.94	3.48	5.26	<b>3.30</b>
QUIK-8B	<b>9.51</b>	<b>9.29</b>	<b>4.89</b>	<b>3.33</b>	<b>5.23</b>	3.31

**Outlier-Free Layers.** Finally, we study the effect of keeping multiple linear layers without any outliers. This might help boost end-to-end performance by removing all the outlier-related overheads during the forward pass. (Although, as we show later, these overheads are minor.) Table 5 shows how the accuracy of different models changes when we use different absolute threshold values (shown by  $T$ ), extracted using a linear search, for the outliers. We con-

Model	$T$	LLaMA2-70B	Falcon-180B
FP16	-	3.2	3.30
	0	3.74 (0)	3.61 (0)
	2.0	3.75 (10)	3.61 (3)
	3.0	3.85 (30)	3.61 (4)
	4.0	5.15 (58)	3.72 (14)
QUIK-4B	8.0	5.92 (219)	3.73 (115)

Table 5. Study of zero outlier setting on WikiText2 using 256 outliers. We use zero outliers when the maximum of scale is less than threshold  $T$ . For each experiment, the number of linear layers with zero outliers is written in parentheses.

clude that there is no universal threshold across all models, which would preserve accuracy across all models. For example, Falcon-180B can achieve reasonable accuracy even if 24% of the linear layers (115 out of 480) contain zero outliers. However, this is not the case for smaller models: LLaMA2-70B can recover accuracy with up to 5% of the linear layers (30 out of 560) having zero QUIK outliers. We provide additional experiments in Appendix D.

**4.2 Performance Analysis**

We now examine the performance of the QUIK implementation by evaluating different aspects of our kernel. We use PyTorch/1.13, CUDA/11.8, Huggingface Transformers/4.34. We run all our experiments on RTX 3090 GPUs as our main goal is to accelerate LLM inference on commodity GPUs. Appendix G shows similar results on RTX 3080 GPUs.

**Peak Memory Usage.** First, we assess the memory usage of our quantized models. In Table 6, we evaluate the peak memory usage across different configurations for the OPT and LLaMA-2 families. For OPT-66B, the QUIK-8B and QUIK-4B models demonstrate peak memory reductions of approximately 47% (compared to the ideal 50% reduction) and 74% (compared to the ideal 75% reduction), respectively. For the LLaMA2-70B model, the reductions are 32% for QUIK-8B and 67% for QUIK-4B. This is because we keep the down-projection in 8-bits and use additional out-

Model	OPT			LLaMA-2		
	13B	30B	66B	7B	13B	70B
Baseline	30.5	67.4	162.1	14.9	28.0	147.1
QUIK-8B	16.1	39.3	81.2	14.6	25.2	99.3
QUIK-4B	<b>10.7</b>	<b>24.6</b>	<b>45.1</b>	<b>7.1</b>	<b>12.1</b>	<b>49.1</b>

Table 6. Peak memory usage (in GB) in an end-to-end benchmark. In total, the outliers take 2.71 GB and 4.06 GB for OPT-66B and LLaMA2-70B models respectively.

liers. Additional overheads come from auxiliary buffers, which differ for various layer sizes.

**Ideal and Layer-wise Speedups.** Next, we evaluate the ideal speedups, as well as the actual speedups we measure in each Transformer block separately. The results in Figure 3 depict “ideal” computational power for layer-wise matrix multiplications at different precision levels, without taking into account any quantization/dequantization overheads. Here, we focus on realizable speedups when executing Algorithm 1, which includes mixed-precision multiplication as well as compression and decompression operations.

In Figure 7, we compare the layer-wise performance of quantized linear layers (QUIK-4B uses 256 outliers per layer) relative to FP16, for a full implementation of our algorithm. The matrix sizes correspond to layers in LLaMA models. We observe that QUIK-4B can achieve slightly higher than 4x speedup on large layers and over 2x on smaller ones. Thus, the speedups of raw low-precision matmul speedups can partially “hide” the overheads of QUIK.

**End-to-end speedups.** Finally, we also demonstrate the end-to-end speedup benefits of QUIK models. For this purpose, we integrate QUIK into the widely used HuggingFace PyTorch implementation, by replacing linear layers with 4-bit (and 8-bit) QUIK re-implementations. For the LLaMA model, we use FlashAttention (Dao et al., 2022) for all models (including FP16). The number of outliers in QUIK-4B is set to 256 except for the special case of down projection layers in LLaMA and FC2 in the Falcon models, which we quantize to 8 bits with more than 600 outliers.

In Figure 9, we compare the throughput improvements of prefill passes (for single batches with 2048 tokens) for quantized models, relative to the corresponding FP16 version. The bar plot shows throughput improvements of QUIK-4B compared to FP16. The annotations to the baseline represent its actual throughput values in our experiments. For instance, OPT-66B using FP16 linear layers achieved 439 tokens/s whereas the same model inference with QUIK-4B linear layers resulted in 1343 tokens/s. This shows that, in addition to a close to 4x memory reduction, which reduces the number of required GPUs for inference, QUIK

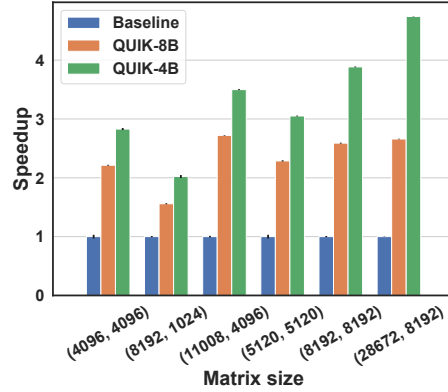


Figure 7. Layer-wise speedups on a single RTX3090 for different layer sizes and compression types. QUIK-4B with 256 outliers, QUIK-8B without outliers.

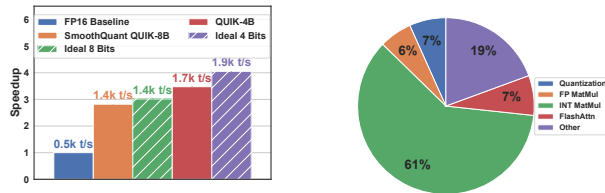


Figure 8. Performance results and overhead breakdown on LLaMA2-70B on a machine with 8x RTX 3090 GPUs. **Left:** Speedup vs. FP16 and vs. an ideal implementation, without overheads, for 4-bit and 8-bit QUIK kernels with absolute throughput values. **Right:** Performance breakdown of end-to-end inference benchmark for QUIK-4B with outliers in terms of MatMul time vs. quantization overheads.

also achieves up to 3.4x higher throughput relative to FP16, with the biggest improvements attained on the largest models (LLaMA2-70B), where the relative impact of overheads is lowest. The memory reduction is important in the Falcon inference case: we were not able to run Falcon-180B in full precision on 8xRTX3090 GPUs, as the max memory peak of the model is more than 360GB. However, QUIK-4B allows us to run full inference of this 180B model on a single server resulting in 542 tokens/second. Therefore, we estimated speedups for the FP16 180B model in Figure 9(c) based on the runtime of a single Transformer block.

We emphasize that the speedups in our end-to-end experiments are exclusively through QUIK accelerated linear layers. All other functions are precisely the same. As shown in Figure 8 (Right), the overheads from attention, softmax, or layernorm operations become significant when a large fraction of the computation occurs in 4-bit precision.

**Outlier Performance Costs.** To illustrate the performance implications of supporting outliers, in Figure 8 (left) we pro-



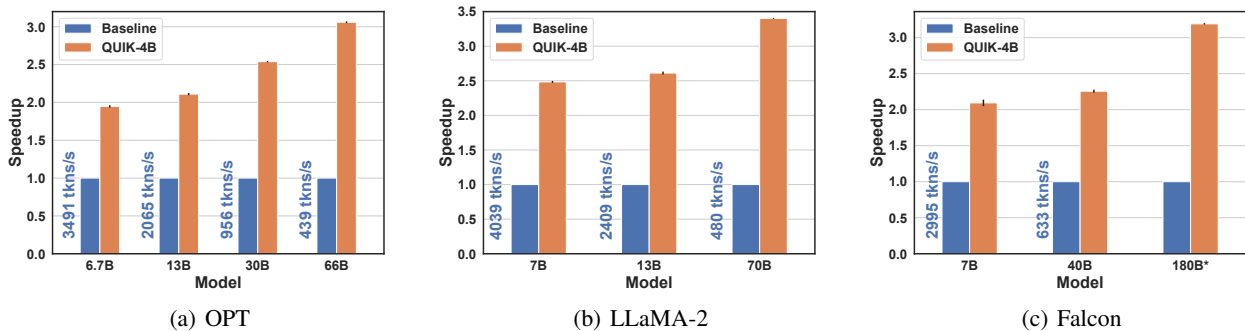


Figure 9. End-to-end inference speedups for QUIK-4B with outliers relative to the FP16 baseline, on NVIDIA RTX 3090 GPUs. Falcon-180B results are from single Transformer block inference benchmark.

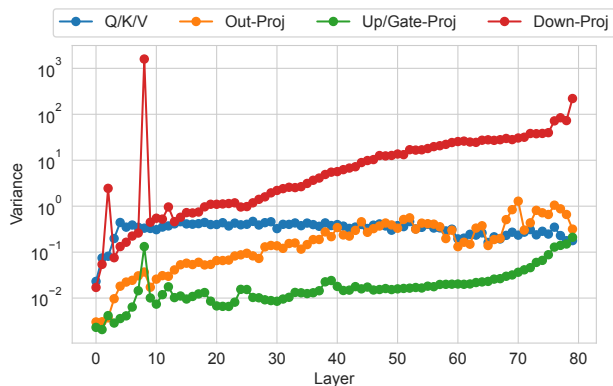


Figure 10. The variance of the inputs in different layers of LLaMA2-70B. The "Down-Proj" layers have significantly larger variances, resulting in poor 4-bit quantization.

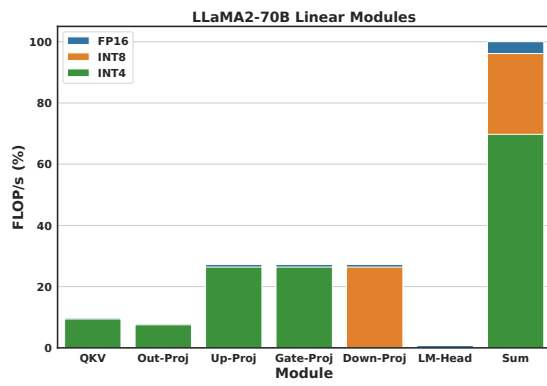


Figure 11. FLOP/s analysis of the LLaMA2-70B linear layers with QUIK. We use 3.125% outliers (256 outliers in all layers and 896 for the down-projection layer) and 2048 sequence length.

vide end-to-end speedups for variants of the HuggingFace integration where we directly use 8-bit and 4-bit kernels, without preserving accuracy (Ideal 8-bit and 4-bit), relative to our accuracy-preserving QUIK implementations.

We observe that the 8-bit implementation provides close to ideal speedups, reducing the number of GPUs from 7 to 5. QUIK-4B (taking outliers into account) performs  $\approx 15\%$  better, further reducing the number of required GPUs to 3, using less than 50 GB of GPU memory. The performance impact of outlier selection (hence mixed precision matrix multiplication) and selective 8-bit quantization (for down-projection MLP layer) is shown in the comparison with Ideal 4-bit. QUIK-4B is within 15% of Ideal 4-bit performance. (However, it is currently not known how a model with weights and activations in 4 bits could recover accuracy.) The justification for this performance impact is provided in Figure 8 (right), where we break down the per-operation overheads for LLaMA2-70B inference. Specifically, we observe here and in Figure 6 that the overheads of quantization and full precision multiplication can take

up a large fraction of the overall operation time, especially for smaller matrices. This illustrates the trade-offs between performance and accuracy for a specific model.

### 4.3 Ablation Studies

We now provide in-depth examples for using QUIK on two large models: LLaMA2-70B, and Falcon-180B. The former model is important as it shows high performance across different tasks (Touvron et al., 2023). The latter is the largest openly-available GPT-type model.

#### 4.3.1 Case Study 1: LLaMA2-70B

First, we study the FLOP breakdown across precisions using QUIK-4B on LLaMA2-70B. Next, we study the effect of key parameters of QUIK: 8-bit Down-Projection, and Outlier Counts. We provide additional ablation in Appendix B.

**8-bit Down-Projection.** Within the MLP module of the LLaMA2-70B model, three linear layers are present, re-

ferred to as "Up-Proj", "Gate-Proj", and "Down-Proj". "Up-Proj" and "Gate-Proj" share an input (MLP input) and apply their respective linear transformations to it. Subsequently, the output of "Gate-Proj" is subjected to a SiLU activation function. Lastly, the input for the "Down-Proj" layer is constructed by taking the Hadamard product of the outputs from "Up-Proj" and "Gate-Proj".

LLaMA-2	7B	13B	70B
Baseline	5.47	4.88	3.20
QUIK-4B	5.84	5.28	3.74
4-bit Down-Proj	8.87	7.78	6.91

Table 7. Ablation for keeping the down-projection layer in 4-bits.

Figure 10 shows the variance of the input across various layers in LLaMA2-70B, which we use as a guide to choose both the number of outliers and the set of layers to be executed in 8 bit precision. Specifically, it can be observed that the "Down-Proj" layers have large input variance, mainly due to the Hadamard product of the previous two outputs, resulting in poor accuracy for 4-bit quantization. To address this, we employ *8-bit quantization* for both the weights and activations within the "Down-Proj" layers of LLaMA2 models. Table 7 shows that keeping the down-projection layers in 8-bit is critical for high accuracy on LLaMA2, as it improves perplexity by > 2 points, across all models.

**FLOP/s Analysis.** Figure 11 shows the percentage of the FLOP/s we keep in each precision (INT4 for base weights, FP16 for outliers, and INT8 for down-projection layers) in LLaMA2-70B. More precisely, for 256 outliers, we perform  $\approx 70\%$  of the operations in 4-bit and  $\approx 27\%$  using 8-bits.

Method	Outliers	Down-Proj Outliers	WikiText2 (PPL)
Baseline	-	-	3.20
QUIK-4B	128	448	3.80
	256	896	3.74
	512	1792	3.67
	1024	3584	3.62

Table 8. Ablation study of different outlier numbers in QUIK for the LLaMA2-70B model.

**Outlier Count.** Finally, we look at how different outlier counts affect the WikiText2 score for the LLaMA2-70B model. In Table 8, we observe that increasing the outliers from 128 to 1024 results in a 0.2 perplexity improvement. We also adjusted the outliers for down-projection layers, ensuring there are 3.5x times more than the other linear layers, to match input size. Our results show that using 256 outliers is already a good choice for our experiments. Using additional outliers does not significantly improve accuracy.

Precision	Sparsity	Dense Layers	WikiText2 (PPL)	Mem. Peak (rel to FP16)
FP16	0%	All	3.30	100%
	2:4	None	6.13	-
QUIK-4B	0%	All	3.61	38 %
	2:4	None	6.62	25%
	2:4	Attn. Blocks	6.34	26%
	2:4	MLP Blocks	<b>3.93</b>	36%

Table 9. Accuracy results for quantized + 2:4 sparsified on Falcon-180B. For the quantized experiments, we apply quantization on all layers with 256 outliers but keep some of the layers in dense (mentioned in the Table). By memory peak we mean the maximal amount of allocated memory (in GB) during the inference of a single Transformer block.

### 4.3.2 Case Study 2: Falcon-180B

In this section, we revisit applying QUIK to Falcon-180B, the largest GPT-style openly-available model. The model requires  $\approx 365$ GB of GPU memory for the inference, which makes it impossible to run inference on a GPU server with 8x RTX3090 nodes (192 GB memory), illustrating the importance of reducing the memory footprint of this model.

The results in Tables 2 and 5, and Figure 9 already presented accuracy and performance results for this model for QUIK variants. Here, we investigate leveraging the hardware-supported 2:4 sparse + INT4 format by combining QUIK with 2:4 sparsity for this model.

**Joint INT-4 Quantization and 2:4 Sparsification.** A simple solution for pushing the limits of the model compression is to sparsify the already quantized model (or vice-versa). However, this results in high accuracy drops. Instead, we extend the SparseGPT algorithm (Frantar & Alistarh, 2023) to support our outlier scheme to jointly quantize and sparsify the model, while keeping the outlier features in dense FP16. In Table 9, we present the results of quantizing all layers, but selectively keep certain layer types dense. Specifically, we found that one-shot pruning of the weights in the attention blocks to the 2:4 pattern throughout all layers largely preserves accuracy, leading to small memory gains. We present 8-bit results in the same setting in Appendix E.

## 5 CONCLUSION AND FUTURE WORK

We presented a hybrid quantization scheme called QUIK, executing a large majority of inference computation in 4-bit precision, with efficient GPU support. We have shown significant speedups using QUIK across several LLM types, on commodity hardware. In future work, we plan to examine a unified implementation which would support both single-token and multi-token inference on top of QUIK weights, integration with speculative decoding (Leviathan et al., 2023), and additional models.

## REFERENCES

- Boratko, M., Padigela, H., Mikkilineni, D., Yuvraj, P., Das, R., McCallum, A., Chang, M., Fokoue-Nkoutche, A., Kanipathi, P., Mattei, N., et al. A systematic classification of knowledge, reasoning, and context within the ARC dataset. *arXiv preprint arXiv:1806.00358*, 2018.
- Choi, J., Wang, Z., Venkataramani, S., Chuang, P. I.-J., Srinivasan, V., and Gopalakrishnan, K. Pact: Parameterized clipping activation for quantized neural networks. *arXiv preprint arXiv:1805.06085*, 2018.
- Dao, T., Fu, D. Y., Ermon, S., Rudra, A., and Ré, C. FlashAttention: Fast and memory-efficient exact attention with io-awareness. *arXiv preprint arXiv:2205.14135*, 2022.
- Dettmers, T. and Zettlemoyer, L. The case for 4-bit precision: k-bit inference scaling laws. *arXiv preprint arXiv:2212.09720*, 2022.
- Dettmers, T., Lewis, M., Belkada, Y., and Zettlemoyer, L. LLM.int8(): 8-bit matrix multiplication for transformers at scale. *Advances in Neural Information Processing Systems 35: Annual Conference on Neural Information Processing Systems 2022, NeurIPS 2022*, 2022.
- Dettmers, T., Svirschevski, R., Egiazarian, V., Kuznedelev, D., Frantar, E., Ashkboos, S., Borzunov, A., Hoefler, T., and Alistarh, D. Spqr: A sparse-quantized representation for near-lossless llm weight compression. *arXiv preprint arXiv:2306.03078*, 2023.
- Esser, S. K., McKinstry, J. L., Bablani, D., Appuswamy, R., and Modha, D. S. Learned step size quantization. *arXiv preprint arXiv:1902.08153*, 2019.
- Frantar, E. and Alistarh, D. Sparsegpt: Massive language models can be accurately pruned in one-shot. 2023.
- Frantar, E., Ashkboos, S., Hoefler, T., and Alistarh, D. Gptq: Accurate post-training quantization for generative pre-trained transformers. *arXiv preprint arXiv:2210.17323*, 2022.
- Gao, L., Biderman, S., Black, S., Golding, L., Hoppe, T., Foster, C., Phang, J., He, H., Thite, A., Nabeshima, N., et al. The pile: An 800gb dataset of diverse text for language modeling. *arXiv preprint arXiv:2101.00027*, 2020.
- Gao, L., Tow, J., Biderman, S., Black, S., DiPofi, A., Foster, C., Golding, L., Hsu, J., McDonnell, K., Muennighoff, N., et al. A framework for few-shot language model evaluation. *Version v0. 0.1. Sept*, 2021.
- Kim, S., Hooper, C., Gholami, A., Dong, Z., Li, X., Shen, S., Mahoney, M. W., and Keutzer, K. Squeezellm: Dense-and-sparse quantization. *arXiv preprint arXiv:2306.07629*, 2023.
- Lee, C., Jin, J., Kim, T., Kim, H., and Park, E. Owq: Lessons learned from activation outliers for weight quantization in large language models. *arXiv preprint arXiv:2306.02272*, 2023.
- Leviathan, Y., Kalman, M., and Matias, Y. Fast inference from transformers via speculative decoding. In *International Conference on Machine Learning*, pp. 19274–19286. PMLR, 2023.
- Li, Q., Zhang, Y., Li, L., Yao, P., Zhang, B., Chu, X., Sun, Y., Du, L., and Xie, Y. Fptq: Fine-grained post-training quantization for large language models. *arXiv preprint arXiv:2308.15987*, 2023.
- Lin, J., Tang, J., Tang, H., Yang, S., Dang, X., and Han, S. Awq: Activation-aware weight quantization for llm compression and acceleration. *arXiv preprint arXiv:2306.00978*, 2023.
- Merity, S., Xiong, C., Bradbury, J., and Socher, R. Pointer sentinel mixture models. *arXiv preprint arXiv:1609.07843*, 2016.
- NVIDIA. Nvidia nsight compute. URL <https://developer.nvidia.com/nsight-compute>.
- NVIDIA. Nvidia cutlass library, 2023. URL <https://github.com/NVIDIA/cutlass/>.
- Paszke, A., Gross, S., Massa, F., Lerer, A., Bradbury, J., Chanan, G., Killeen, T., Lin, Z., Gimelshein, N., Antiga, L., et al. Pytorch: An imperative style, high-performance deep learning library. *Advances in neural information processing systems*, 32, 2019.
- Radford, A., Wu, J., Child, R., Luan, D., Amodei, D., and Sutskever, I. Language models are unsupervised multitask learners. *OpenAI blog*, 1(8):9, 2019.
- Raffel, C., Shazeer, N., Roberts, A., Lee, K., Narang, S., Matena, M., Zhou, Y., Li, W., and Liu, P. Exploring the limits of transfer learning with a unified text-to-text transformer. *Journal of Machine Learning Research*, 21 (140):1–67, 2020.
- Sakaguchi, K., Bras, R. L., Bhagavatula, C., and Choi, Y. Winogrande: An adversarial winograd schema challenge at scale. *Communications of the ACM*, 64(9):99–106, 2021.
- Shao, W., Chen, M., Zhang, Z., Xu, P., Zhao, L., Li, Z., Zhang, K., Gao, P., Qiao, Y., and Luo, P. Omniquant: Omnidirectionally calibrated quantization for large language models, 2023.
- Tata, S. and Patel, J. M. PiQA: An algebra for querying protein data sets. In *International Conference on Scientific and Statistical Database Management*, 2003.

- TII UAE. The Falcon family of large language models. <https://huggingface.co/tiiuae>, May 2023.
- Touvron, H., Martin, L., Stone, K., Albert, P., Almahairi, A., Babaei, Y., Bashlykov, N., Batra, S., Bhargava, P., Bhosale, S., et al. Llama 2: Open foundation and fine-tuned chat models. *arXiv preprint arXiv:2307.09288*, 2023.
- Wolf, T., Debut, L., Sanh, V., Chaumond, J., Delangue, C., Moi, A., Cistac, P., Rault, T., Louf, R., Funtowicz, M., et al. Huggingface’s transformers: State-of-the-art natural language processing. *arXiv preprint arXiv:1910.03771*, 2019.
- Xiao, G., Lin, J., Seznec, M., Demouth, J., and Han, S. Smoothquant: Accurate and efficient post-training quantization for large language models. *arXiv preprint arXiv:2211.10438*, 2022.
- Yuan, Z., Niu, L., Liu, J., Liu, W., Wang, X., Shang, Y., Sun, G., Wu, Q., Wu, J., and Wu, B. Rptq: Reorder-based post-training quantization for large language models. *arXiv preprint arXiv:2304.01089*, 2023.
- Zellers, R., Holtzman, A., Bisk, Y., Farhadi, A., and Choi, Y. Hellaswag: Can a machine really finish your sentence? *arXiv preprint arXiv:1905.07830*, 2019.
- Zhang, S., Roller, S., Goyal, N., Artetxe, M., Chen, M., Chen, S., Dewan, C., Diab, M., Li, X., Lin, X. V., et al. OPT: Open pre-trained transformer language models. *arXiv preprint arXiv:2205.01068*, 2022.



## A FULL OPT ACCURACY RESULTS

Table 10 shows the perplexity results of OPT models. We use symmetric quantization for the weights in all our experiments. The results suggest that in a 4-bit setting, considering outlier features is crucial to preserve the accuracy even in small models (like OPT-1.3b). We note that 256 outliers is equivalent to 12.5% of the 1.3B model’s hidden size (and 2.77% of the 66B model’s hidden size).

Model	OPT-1.3b			OPT-6.7b			OPT-13b			OPT-30b			OPT-66b		
	WIKI	PT	C4	WIKI	PT	C4	WIKI	PT	C4	WIKI	PT	C4	WIKI	PT	C4
Baseline	14.63	16.96	14.72	10.86	13.09	11.74	10.13	12.34	11.20	9.56	11.84	10.69	9.34	11.36	10.28
GPTQ-4B	15.89	18.83	15.90	11.43	13.81	12.21	10.38	12.65	11.41	9.60	12.02	10.83	9.65	11.63	10.56
0 Outliers	15k	9k	10k	10k	9k	9k	9k	12k	9k	12k	13k	17k	12k	13k	10k
64 Outliers	26.259	27.143	22.981	11.473	13.888	12.348	11.031	13.305	11.971	10.283	12.557	11.267	9.851	11.965	10.742
128 Outliers	17.638	19.709	16.799	11.671	13.809	12.314	10.964	13.241	11.894	10.339	12.564	11.279	9.805	11.842	10.653
256 Outliers	17.358	19.525	16.607	11.184	13.811	12.262	10.779	13.175	11.847	10.078	12.465	11.226	9.662	11.793	10.635

Table 10. Perplexity scores of QUIK-4B over various OPT models with different outliers on three datasets: WikiText2 (WIKI), Pen Treebank (PT), and C4. GPTQ-4B only quantizes the weights (using int-4 symmetric quantization) and keeps the activations in FP16.

## B FULL LLAMA-2 ACCURACY RESULTS

Table 11 shows the perplexity of QUIK on LLaMA-2 models. We provide a list of tricks to improve the quality of the model without too much overhead. We found that keeping the down-proj layer in 8 bits can improve the perplexity by about 3 points. Also, we found weight clipping as a cheap and efficient trick for improving the accuracy of QUIK-4B.

LLaMA-2	Down-Proj	Clipping	7B	13B	70B
FP16	W16A16	-	5.47	4.88	3.2
GPTQ-4B	W4A16	-	6.24	5.25	3.68
QUIK-4B	W4A4	-	8.78	7.78	6.91
QUIK-4B	W4A16	-	6.09	5.49	3.98
QUIK-4B	W4A8	-	6.11	5.5	4.0
QUIK-4B	W8A8	-	5.98	5.37	3.87
QUIK-4B	W8A8	✓	5.84	5.28	3.74

Table 11. LLaMA-2 perplexity results on WikiText2 using 256 outliers. We apply clipping only during the weight quantization.

## C FULL INT-8 ACCURACY RESULTS

Table 12 shows QUIK-8B comparison against SmoothQuant on the WikiText2 dataset. We use per-token (per-column) quantization for the activations (weights) in SmoothQuant and only apply the quantization on the linear layers (which is the case for QUIK also). We exclude the Falcon-7B model as this model has a single layer-norm for both MLP and Attention blocks and it is not clear how the weights of the FC1 and KQV will be updated in the SmoothQuant algorithm.

## D ZERO-OUTLIER FULL RESULTS

Table 13 shows the results of keeping different numbers of layers without outliers for different models.

**QUIK: Towards End-to-end 4-Bit Inference on Generative Large Language Models**

Model	OPT					LLaMA-2			Falcon	
	1.3b	6.7B	13B	30B	66B	7B	13B	70B	40B	180B
FP16	14.63	10.84	10.13	9.56	9.34	5.47	4.88	3.20	5.23	3.30
SmoothQuant	14.70	10.89	10.37	9.59	9.80	5.58	4.94	3.48	5.26	<b>3.30</b>
QUIK-8B	<b>14.62</b>	<b>10.84</b>	<b>10.13</b>	<b>9.51</b>	<b>9.29</b>	<b>5.48</b>	<b>4.89</b>	<b>3.33</b>	<b>5.23</b>	3.31

Table 12. Accuracy results for 8bit models on WikiText2. We use 256 outliers in QUIK experiments. Following the SmoothQuant paper, we use  $\alpha = 0.8$  hyperparameter for LLaMA-2 models and  $\alpha = 0.5$  for OPT and Falcon families.

Model	T	LLaMA-2			Falcon		
		7B	13B	70B	7B	40B	180B
FP16	-	5.47	4.88	3.2	6.59	5.23	3.30
QUIK-4B	0	5.84 (0)	5.28 (0)	3.74 (0)	6.90 (0)	5.46 (0)	3.61 (0)
	2.0	5.91 (5)	5.33 (3)	3.75 (10)	6.90 (3)	5.46 (1)	3.61 (3)
	3.0	6.09 (11)	5.34 (8)	3.85 (30)	6.91 (14)	5.46 (2)	3.61 (4)
	4.0	6.13 (21)	5.36 (17)	5.15 (58)	6.93 (27)	10.56 (8)	3.72 (14)
	8.0	12.93 (55)	21.85 (66)	5.92 (219)	6.94 (57)	10.61 (33)	3.73 (115)

Table 13. Study of zero outlier setting on WikiText2 using 256 outliers. We use zero outliers when the maximum of scale is less than threshold **T**. For each experiment, the number of linear layers with zero outliers is written in parentheses.

**E 2:4 SPARSITY + INT8 QUANTIZATION**

Table 14 shows the accuracy results of applying QUIK-8B with 2:4 sparsity across all models. The results suggest that the main accuracy drop is from introducing 2:4 sparsity to the weight matrices and keeping some of the layers in dense is crucial to preserve the accuracy (See section 4.3.2).

Model	Sparsity	OPT					LLaMA-2			Falcon		
		1.3b	6.7B	13B	30B	66B	7B	13B	70B	7B	40B	180B
FP16	0%	14.63	10.84	10.13	9.56	9.34	5.47	4.88	3.20	6.59	5.23	3.30
SparseGPT	2:4	24.08	14.15	12.93	10.93	10.08	10.97	8.78	5.70	12.33	12.33	6.13
QUIK-8B	0%	14.62	10.84	10.13	9.51	9.29	5.48	4.89	3.33	6.59	5.23	3.31
	2:4	22.69	14.59	12.87	11.06	10.24	11.07	8.66	5.89	11.07	8.09	6.19

Table 14. WikiText2 accuracy results for applying 2:4 sparsity with QUIK-8B. We use 256 outliers in all experiments.

**F FALCON PERFORMANCE BENCHMARK**

We also explore the performance improvements of Falcon (TII UAE, 2023) models. The 8xRTX3090 machine contains around 190GB GPU memory which is not enough to run fp16 model inference.

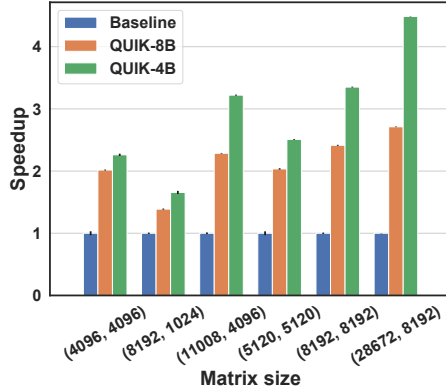


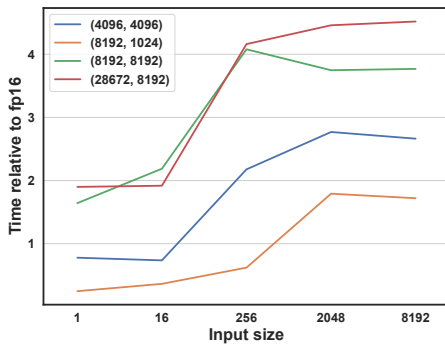
Figure 12. Layer-wise speedups on a single RTX3080 for different layer sizes and compression types. QUIK-4B with 256 outliers, QUIK-8B without outliers.

### G PERFORMANCE ON RTX3080 GPUS

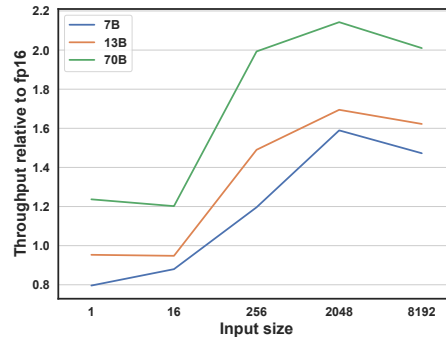
To validate the performance of QUIK in other types of GPUs we conducted benchmarks on RTX3080 GPUs. The results are presented in Figure 12. We can see that QUIK-4B still can get more than 4x speedup on another type of GPU.

### H PERFORMANCE AT DIFFERENT SEQUENCE SIZES

We mainly focus our work on the “prefill” cases with large sequence sizes (in all our experiments sequence size is equal to 2048). In this section we explore the performance of the QUIK-4B with other input sequence sizes. In Figures 13(a) and 13(b) we vary input size from 1 to 8k. In the first experiment (Figure. 13(a)) we ran layer-wise benchmark, in the second (Figure 13(b)) we ran inference of a single Transformer block (on a single GPU). We see that at small input sequence sizes QUIK is noticeably slower for smaller layer size and models. It can be explained by the fact that the gains of low precision matrix multiplication at this scale can not compensate the quantization overheads. However, at large layer and model sizes QUIK has up to 2x speedup even with single token input. In case of the large input sequences we see that performance decreases meaning that low precision matrix multiplication saturates at this scale.



(a) Layerwise Performance.



(b) LLaMA Block performance.

Figure 13. Relative performance of QUIK-4B with outliers for different sequence sizes (batch size = 1) on RTX3090 GPU

### I PERFORMANCE WITH VARIOUS OUTLIER NUMBER

In this section we explore the effect of outliers numbers on the QUIK performances. Figure 14 suggests that the timing of QUIK matmul stays the same across all layer sizes for all non-zero outlier numbers. The zero outliers case superiority can be explained by the fact that it does not have additional full precision matrix multiplication and input data movements. However, these results show that QUIK allow increase the outlier number without performance sacrifices which is crucial

for the accuracy recovery, as we discussed in the Section 4.3.1.

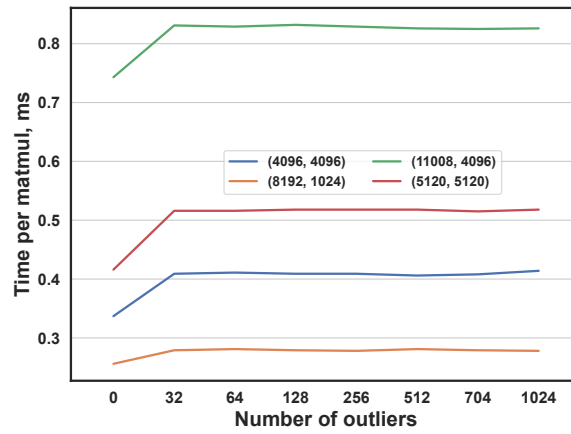


Figure 14. Timing results for different QUIK-4B layers sizes with various number of outliers on RTX3090 GPU.